Programmable two-dimensional optical fractional Fourier processor

José A. Rodrigo, Tatiana Alieva and María L. Calvo

Universidad Complutense de Madrid, Facultad de Ciencias Físicas,Ciudad Universitaria s/n, Madrid 28040, Spain.

jarmar@fis.ucm.es

Abstract: A flexible optical system able to perform the fractional Fourier transform (FRFT) almost in real time is presented. In contrast to other FRFT setups the resulting transformation has no additional scaling and phase factors depending on the fractional orders. The feasibility of the proposed setup is demonstrated experimentally for a wide range of fractional orders. The fast modification of the fractional orders, offered by this optical system, allows to implement various proposed algorithms for beam characterization, phase retrieval, information processing, etc.

OCIS codes: (070.2590) Fourier transforms; (120.4820) Optical systems; (200.4740) Optical processing; (140.3300) Laser beam shaping

References

1. H. M. Ozaktas, Z. Zalevsky, and M. A. Kutay, *The Fractional Fourier Transform with Applications in Optics and Signal Processing* (John Wiley&Sons, NY, USA, 2001).
2. D. F. McAlister, M. Beck, L. Clarke, A. Mayer, and M. G. Raymer, "Optical phase retrieval by phase-space tomography and fractional-order Fourier transforms," Opt. Lett. **20**, 1181–1183 (1995). URL http://ol.osa.org/abstract.cfm?URI=ol-20-10-1181.
3. J. A. Rodrigo, T. Alieva, and M. L. Calvo, "Optical system design for orthosymplectic transformations in phase space," J. Opt. Soc. Am. A **23**, 2494–2500 (2006), http://josaa.osa.org/abstract.cfm?URI=josaa-23-10-2494.
4. D. Mendlovic and H. M. Ozaktas, "Fractional Fourier transform and their optical implementation," J. Opt. Soc. Am. A **10**, 1875–1881 (1993).
5. A. W. Lohmann, "Image rotation, Wigner rotation, and the fractional order Fourier transform," J. Opt. Soc. Am. A **10**, 2181–2186 (1993).
6. A. Sahin, H. M. Ozaktas, and D. Mendlovic, "Optical Implementations of Two-Dimensional Fractional Fourier Transforms and Linear Canonical Transforms with Arbitrary Parameters," Appl. Opt. **37**, 2130–2141 (1998), http://ao.osa.org/abstract.cfm?URI=ao-37-11-2130.
7. I. Moreno, J. A. Davis, and K. Crabtree, "Fractional Fourier transform optical system with programmable diffractive lenses," Appl. Opt. **42**, 6544–6548 (2003).
8. A. A. Malyutin, "Tunable Fourier transformer of the fractional order," Quantum Electron. **36**, 79–83 (2006).
9. I. Moreno, C. Ferreira, and M. M. Sánchez-López, "Ray matrix analysis of anamorphic fractional Fourier systems," J. Opt. A: Pure and Applied Optics **8**, 427–435 (2006), http://stacks.iop.org/1464-4258/8/427.
10. J. A. Rodrigo, T. Alieva, and M. L. Calvo, "Gyrator transform: properties and applications," Opt. Express **15**, 2190–2203 (2007), http://www.opticsexpress.org/abstract.cfm?URI=oe-15-5-2190.
11. J. A. Rodrigo, T. Alieva, and M. L. Calvo, "Experimental implementation of the gyrator transform," J. Opt. Soc. Am. A **24**, 3135–3139 (2007), http://josaa.osa.org/abstract.cfm?URI=josaa-24-10-3135.
12. G. Nemes and A. E. Seigman, "Measurement of all ten second-order moments of an astigmatic beam by use of rotating simple astigmatic (anamorphic) optics," J. Opt. Soc. Am. A **11**, 2257–2264 (1994).
13. J. A. Rodrigo, "First-order optical systems in information processing and optronic devices," Ph.D. thesis, Universidad Complutense de Madrid (2008).
14. T. Alieva and M. J. Bastiaans, "Orthonormal mode sets for the two-dimensional fractional Fourier transformation," Opt. Lett. **32**, 1226–1228 (2007), http://ol.osa.org/abstract.cfm?URI=ol-32-10-1226.

#105474 - $15.00 USD Received 18 Dec 2008; revised 27 Jan 2009; accepted 13 Feb 2009; published 16 Mar 2009

15. A. Jesacher, A. Schwaighofer, S. Fürhapter, C. Maurer, S. Bernet, and M. Ritsch-Marte, "Wavefront correction of spatial light modulators using an optical vortex image," Opt. Express **15**, 5801–5808 (2007), http://www.opticsexpress.org/abstract.cfm?URI=oe-15-9-5801.
16. D. Mendlovic, R. G. Dorsch, A. W. Lohmann, Z. Zalevsky, and C. Ferreira, "Optical illustration of a varied fractional Fourier-transform order and the Radon—Wigner display," Appl. Opt. **35**, 3925–3929 (1996), http://ao.osa.org/abstract.cfm?URI=ao-35-20-3925.

1. Introduction

The fractional Fourier transform (FRFT) plays an important role in digital and optical information processing. In particular, it is a useful tool for beam characterization, filtering, phase space tomography, phase retrieval, encryption, etc. [1, 2]. The FRFT of a two-dimensional function $f(\mathbf{r}_i)$ for parameters γ_x and γ_y, which are known as transformation angles, is defined as

$$F^{\gamma_x,\gamma_y}(\mathbf{r}_o) = \frac{\exp\left[i(\gamma_x+\gamma_y)/2\right]}{i\sqrt{\sin\gamma_x \sin\gamma_y}} \iint f(x_i,y_i)\, \exp\left\{i\pi\left[(x_o^2+x_i^2)\cot\gamma_x - 2x_i x_o \csc\gamma_x\right]\right\} \times \exp\left\{i\pi\left[(y_o^2+y_i^2)\cot\gamma_y - 2y_i y_o \csc\gamma_y\right]\right\} \mathrm{d}x_i \mathrm{d}y_i, \quad (1)$$

where $\mathbf{r}_{i,o} = (x_{i,o}, y_{i,o})$ are the input and output spatial coordinates, respectively [1]. Note that the kernel of FRFT is separable with respect to x and y coordinates. For angles $\gamma_x = \gamma_y = 0$ the FRFT corresponds to the identity transformation, whereas for $\gamma_x = 0$ and $\gamma_y = \pi$ it reduces to image reflection. Meanwhile for $\gamma_x = \gamma_y = \pi/2$ the Fourier transform is obtained. The cases $\gamma_x = \gamma_y = \gamma$ and $\gamma_x = -\gamma_y = \gamma$ correspond to the symmetric and antisymmetric FRFTs, respectively [3]. Therefore the FRFT(γ_x, γ_y) can be understood as a generalization of the Fourier transform. It is usual to define the transformation angle as $\gamma = q\pi/2$, where q is called fractional order. For instance, the order $q = 4$ leads to the self-imaging case meanwhile $q = -1$ corresponds to the inverse Fourier transform. The properties and applications of the FRFT are discussed in detail for example in [1].

In 1993, Mendlovic and Ozaktas introduced the optical FRFT when they analyzed gradient index (GRIN) fiber [4]. In the same year, Lohmann proposed that FRFT could be realized by using conventional lens system [5]. A general treatment of optical systems performing the FRFT was realized by Sahin et al. in 1998 [6], in which the fractional orders can be changed independently. Nevertheless all these systems are not flexible since in order to vary the transformation angle value the distances between lens and input−output planes have to be changed. The most applications such as adaptive filtering, phase space tomography, beam characterization, etc. require a fast and accurate variation of the transformations angles. In 2003 the first optical setup for FRFT based on programmable lenses implemented by a spatial light modulator (SLM) was developed [7]. Alternatively in 2006 Malyutin [8] designed a system for the FRFT able to change the fractional angles by the proper rotation of cylindrical lenses. In the same year, Moreno et al. [9] also proposed a FRFT system based on cylindrical lenses without moving the input and output planes. These optical systems permit relatively easy to modify the fractional order but the resulting field amplitude is affected by an additional scaling depending on the transformation parameter, that in many cases is not desirable.

Recently we have designed lens based optical systems able to perform attractive operations such as image rotation, FRFT and the gyrator transform (GT), [3]. These setups have the following advantages: *i*) distances between lenses and input−output planes are fixed; *ii*) the change of the transformation parameters is only achieved by means of power variation of the lenses; *iii*) the change of transformation parameters does not produce additional scaling of the transformed field; *iv*) the number of lenses used in the setup satisfying the above mentioned conditions is minimal. It has been shown that such flexible systems for the FRFT [3] and the GT [10, 11],

#105474 - $15.00 USD Received 18 Dec 2008; revised 27 Jan 2009; accepted 13 Feb 2009; published 16 Mar 2009

contain three generalized lenses. We remind that the generalized lens is an assembled set of centered cylindrical lenses which can be rotated with respect each other in the plane transversal to the propagation direction, [12]. In particular, for the antisymmetric FRFT [3] and the GT [10, 11], optical systems with variable transformation parameters can be constructed applying glass generalized lenses. The variation of the transformation parameter is achieved by the rotation of the cylindrical lenses, which form the generalized lenses. Nevertheless, as we show here, the required generalized lenses can be performed by using SLMs. Then to the advantages mentioned before one can also add the almost real time variation of the transformation angles.

In this work we present the experimental implementation of a programmable optical setup able to perform the FRFT with arbitrary fractional orders which can be tuned continuously. The system feasibility is demonstrated on the example of the transformation of Hermite−Gaussian and Laguerre−Gaussian beams which are eigenfunctions for the symmetric FRFT.

2. Flexible system design for FRFT

The proposed FRFT setup contains three generalized lenses with fixed distance z between them, see Fig. 1(a), where the last lens and first one are identical ($L_3 = L_1$). Each generalized lens, L_1 and L_2, is an assembled set of two crossed (at angle $\pi/2$) cylindrical lenses with variable lens power given by:

$$\begin{aligned} p_{x,y}^{(1)} &= z^{-1}\left(1-\cot\left(\gamma_{x,y}/2\right)/2\right), \\ p_{x,y}^{(2)} &= 2z^{-1}\left(1-\sin\gamma_{x,y}\right), \end{aligned} \tag{2}$$

correspondingly [3]. The graphical representation of the lens power as a function of the transformation angles (denoted as lens operation curve) is displayed in Fig. 1(b) and 1(c) for L_1 and L_2, respectively. From Eq. (2) it follows that this optical setup performs FRFT for the angle interval $\gamma_{x,y} \in [\pi/2, 3\pi/2]$, see Fig. 1(b) and 1(c). This interval is sufficient for a large list of the FRFT applications including adaptive filtering, beam characterization, phase space tomography, etc. Nevertheless, the entire interval $\gamma_{x,y} \in (0, 2\pi)$ can be also covered, due to the relation $F^{\gamma_x+\pi,\gamma_y+\pi}(\mathbf{r}_o) = F^{\gamma_x,\gamma_y}(-\mathbf{r}_o)$.

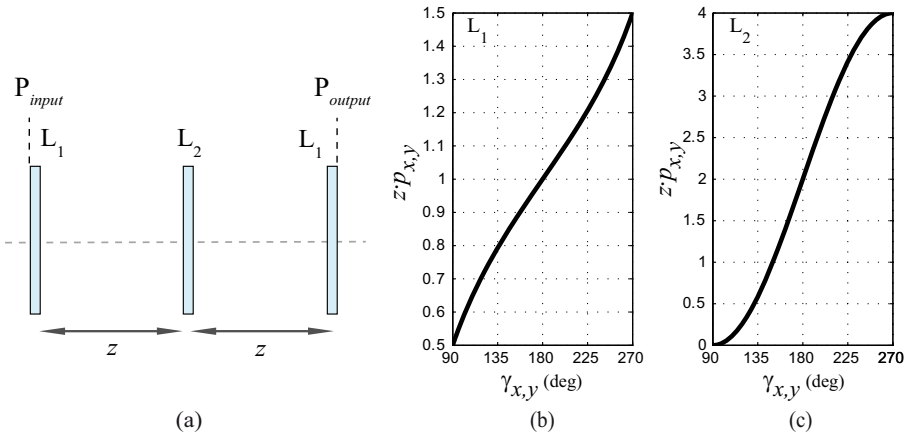

Fig. 1. (a) FRFT optical setup. P_{input} and P_{output} are the input and output planes. The free-space intervals z are fixed. Normalized operation curves $z \cdot p_{x,y}$ for the generalized lenses L_1 and L_2 are displayed in (b) and (c), respectively.

The output complex field amplitude $F^{\gamma_x,\gamma_y}(\mathbf{r}_o)$ can be derived from input signal $f(\mathbf{r}_i)$ apply-

#105474 - $15.00 USD Received 18 Dec 2008; revised 27 Jan 2009; accepted 13 Feb 2009; published 16 Mar 2009

ing the phase modulation function associated with each generalized lens L_j ($j = 1,2$):

$$\Psi_j(x,y) = \exp\left(-\frac{i\pi}{\lambda z} p_x^{(j)} x^2\right) \exp\left(-\frac{i\pi}{\lambda z} p_y^{(j)} y^2\right), \tag{3}$$

and the Fresnel diffraction integral calculation, corresponding to each free-space interval. Then the complex field amplitude at the output plane of the FRFT setup is given by [3, 13]:

$$F^{\gamma_x,\gamma_y}(x_o,y_o) = \frac{1}{2\lambda z\sqrt{\sin\gamma_x \sin\gamma_y}} \iint f_i(x_i,y_i) \exp\left\{\frac{i\pi}{2\lambda z}\left[(x_o^2+x_i^2)\cot\gamma_x - 2x_i x_o \csc\gamma_x\right]\right\}$$
$$\times \exp\left\{\frac{i\pi}{2\lambda z}\left[(y_o^2+y_i^2)\cot\gamma_y - 2y_i y_o \csc\gamma_y\right]\right\} \mathrm{d}x_i \mathrm{d}y_i. \tag{4}$$

The latter expression coincides with the definition of the FRFT [see Eq. (1)] except for a constant phase factor and normalization $s^2 = 2\lambda z$, which is independent of the transformation angles γ_x and γ_y. Notice that the described algorithm is used for the numerical simulation of this FRFT setup.

Since many applications such as beam characterization, phase retrieval, chirp detection, etc., demand the acquisition of the FRFT squared moduli for various angles associated with intensity distributions, the implementation of the third generalized lens ($L_3 = L_1$) is not required. Therefore the optical setup for the measurements of the FRFT power spectra, considered below, consists from only two generalized lenses: L_1 and L_2. The rapid variation of the fractional angles, directly related to the generalized lens powers [Eq. (2)], can be achieved by using SLM for the lens implementation.

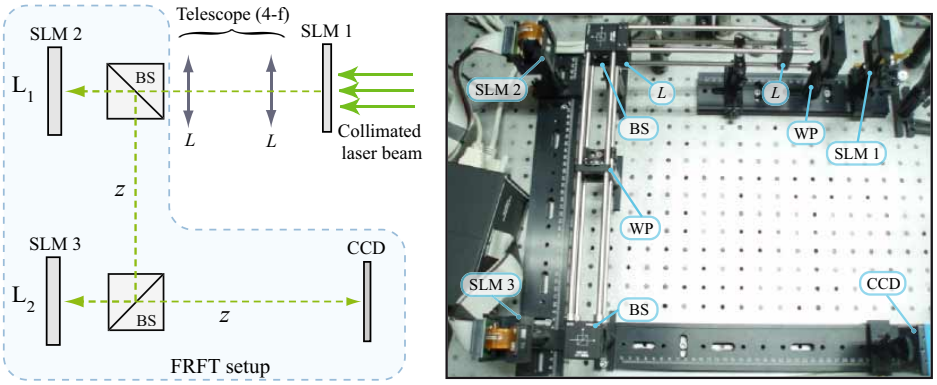

Fig. 2. Experimental setup. The amplitude and phase distributions of the input signal are generated by means of SLM1 (CRL-XGA2, 1024×768 pixels) and SLM2, correspondingly. SLM2 and SLM3 (Holoeye LCR-2500, 1024×768 pixels) implement L_1 and L_2 lens, respectively. Output signal is registered by a CCD camera (XGA, 4.6 μm pixel size). The optical path z is set at 50 cm. SLM performance at phase-only modulation is reached by using a $\lambda/2$ wave plate (WP).

Here we propose the experimental setup for the acquisition of the FRFT power spectra, displayed in Fig. 2, where two reflective SLMs operating in phase-only modulation (SLM2 and SLM3) are used for lens implementation. For the input signal $f(x_i,y_i)$ generation we also apply a transmissive SLM (SLM1) which modulates the amplitude of a collimated Nd:YAG laser beam with wavelength $\lambda = 532$ nm. Thus the amplitude distribution $|f(x_i,y_i)|$ is implemented on SLM1 that is projected on SLM2 by using a 4-f lens system, where its phase distribution

#105474 - $15.00 USD Received 18 Dec 2008; revised 27 Jan 2009; accepted 13 Feb 2009; published 16 Mar 2009

$\arg[f(x_i,y_i)]$ is addressed together with the phase $\arg[\Psi_1(x,y)]$ associated to the first generalized lens. At the distance corresponding to the optical path z (in our case $z=50$ cm) the SLM3 is located, which implements the generalized lens L_2. The intensity distribution of the output signal is registered by a CCD camera that is placed at the distance corresponding to the optical path z from the SLM3, see Fig. 2. Each SLM is connected to the same PC and the alignment between them is reached digitally which is limited by the pixel size (19 μm in our case). Thus position stages for the SLM alignment are not required. We have developed a customized software for the system control able to change the fractional orders at almost real time and to store the measured FRFT power spectra as a video file.

3. Experimental results

In order to test the proposed experimental setup we use as input signals the Hermite−Gaussian (HG)

$$\mathrm{HG}_{m,n}(\mathbf{r};w)=2^{1/2}\frac{H_m\left(\sqrt{2\pi}\frac{x}{w}\right)H_n\left(\sqrt{2\pi}\frac{y}{w}\right)}{\sqrt{2^m m!w}\sqrt{2^n n!w}}\exp\left(-\frac{\pi}{w^2}r^2\right), \tag{5}$$

and Laguerre−Gaussian (LG)

$$\mathrm{LG}^{\pm}_{p,l}(\mathbf{r};w)=w^{-1}\left(\frac{p!}{(p+l)!}\right)^{1/2}\left[\sqrt{2\pi}\left(\frac{x}{w}\pm i\frac{y}{w}\right)\right]^l L_p^l\left(\frac{2\pi}{w^2}r^2\right)\exp\left(-\frac{\pi}{w^2}r^2\right) \tag{6}$$

modes, where: $r^2=x^2+y^2$, H_m is the Hermite polynomial, w is the beam waist, and L_p^l is the Laguerre polynomial with radial index p and azimuthal index l. In contrast to the HG modes, the LG ones are vortex beams which carry Orbital Angular Momentum (OAM): $l\hbar$ per photon. The HG and LG modes are eigenfunctions of the symmetric FRFT [$\gamma_x=\gamma_y=\gamma$, Ec. (4)] for $w=\sqrt{2\lambda z}$ (in our case $w=0.73$ mm). Moreover a HG mode also does not change under the antisymmetric FRFT ($\gamma_x=-\gamma_y=\gamma$), meanwhile a LG mode is transformed into intermediate HG−LG modes with fractional OAM: $l\hbar\sin 2\gamma$, [14].

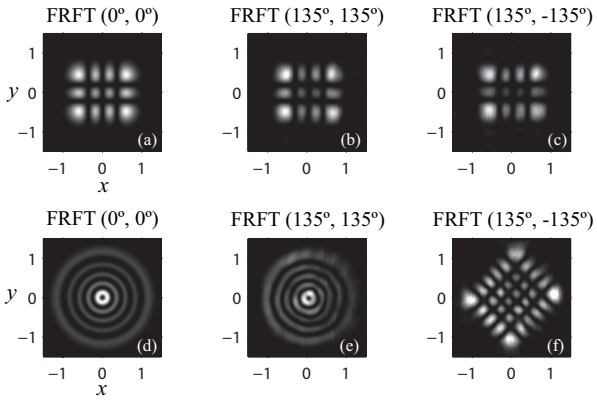

Fig. 3. Input signals $\mathrm{HG}_{3,2}$ (a) and $\mathrm{LG}^{+}_{4,1}$ (d) that coincide with their FRFT$(0^o,0^o)$ for each case. Their transformations under symmetric FRFT(γ,γ) (b) (Media 1) and (e) (Media 2), as well as under antisymmetric FRFT$(\gamma,-\gamma)$ (c) (Media 3) and (f) (Media 4) are displayed, correspondingly. The FRFT operations for angle interval $\gamma\in[90^o,270^o]$ were stored as a video file with 30 fps. Units in axis x and y are in mm.

In particular, applying the antisymmetric FRFT for angles $\gamma=(2k+1)\pi/4$ to the $\mathrm{LG}^{\pm}_{p,l}(\mathbf{r};w)$ mode, where k is an integer whereas $p=\min(m,n)$ and $l=|m-n|$, the $\mathrm{HG}_{m,n}(\mathbf{r};w)$ one (ro-

#105474 - $15.00 USD Received 18 Dec 2008; revised 27 Jan 2009; accepted 13 Feb 2009; published 16 Mar 2009

tated at angle $\pm\pi/4$) is obtained. Therefore it is easy to test the FRFT experimental setup using the HG and LG modes because we know exactly their transformation for any angle. The system characterization has been done with the HG and LG modes for different indices. Here we demonstrate the experimental results, Fig. 3, for $HG_{3,2}$ 3(a) and $LG^{+}_{4,1}$ 3(d) modes.

The symmetric FRFT at angle $\gamma = 135^{o}$ is displayed in Fig. 3(b) and 3(e) for $HG_{3,2}$ and $LG^{+}_{4,1}$, respectively. Meanwhile the antisymmetric FRFT at angle $\gamma = 135^{o}$ is shown in Fig. 3(c) and 3(f) for $HG_{3,2}$ and $LG^{+}_{4,1}$, correspondingly. These transformations have been recorded as video at real time for the angle interval $\gamma \in [90^{o}, 270^{o}]$ with step of 1^{o} and frame rate 30 fps, see Fig. 3. As it has been expected, we observe that the intensity distributions of $HG_{3,2}$ and $LG^{+}_{4,1}$ during the transformation are almost constant except for the antisymmetric FRFT of $LG^{+}_{4,1}$ where intermediate HG−LG modes are obtained.

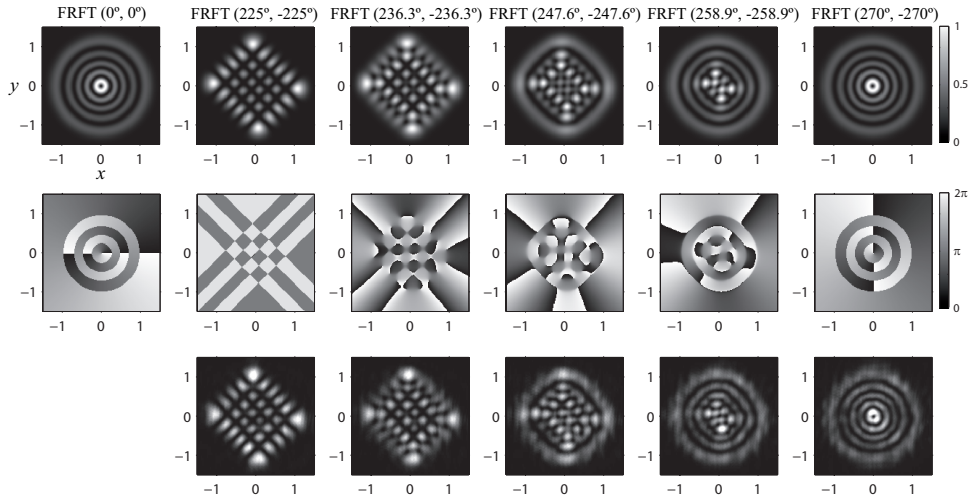

Fig. 4. Numerical simulation (first and second row) and experimental results (third row, Media 4) corresponding to $LG^{+}_{4,1}$ transformation under antisymmetric FRFT$(\gamma, -\gamma)$.

The transformation of $LG^{+}_{4,1}$ mode under antisymmetric FRFT is also displayed in Fig. 4 for $\gamma = 225^{o} + k11.3^{o}$, where $k = 0, ..., 4$. First and second rows (intensity and phase distribution) correspond to numerical simulation of the FRFT setup whereas experimental results are displayed at the third row, see Fig. 4. Notice that the phase distributions here and further correspond to the simulation of the FRFT system with three lenses [see Fig. 1(a)].

As it is demonstrated in Fig. 3 (Media 1−4) and Fig. 4, the resulting transformation has no scaling factors depending on the transformation angles. These results are in good agreement with the theoretical predictions that demonstrates the optical setup feasibility. Nevertheless, it is observed a weak distortion in the intensity distribution during these transformations that we address to discrete structure of the SLM and its dynamic range (256 levels in our case). Moreover, the nonlinear response of the SLM and the deviation from flatness of its reflective surface lead to distortions in phase modulation which could be reduced applying wavefront correction techniques discussed in [15].

In order to demonstrate the FRFT operation for the case $|\gamma_x| \neq |\gamma_y|$ we consider $\left|LG^{+}_{4,1}\right|$ as an input signal. In contrast to the previous input signal $LG^{+}_{4,1}$, the $\left|LG^{+}_{4,1}\right|$ is an image with a constant phase distribution. Let us first consider the symmetric FRFT of $\left|LG^{+}_{4,1}\right|$ for $\gamma = 90^{o} + k22.5^{o}$ with $k = 0, ..., 4$, Fig. 5. Since $\left|LG^{+}_{4,1}\right|$ is not an eigenfunction for the FRFT, as it is

#105474 - $15.00 USD Received 18 Dec 2008; revised 27 Jan 2009; accepted 13 Feb 2009; published 16 Mar 2009

the case for $\mathrm{LG}^{+}_{4,1}$, the intensity distribution is changing with variation of the fractional order. Notice that for FRFT$(90^o, 90^o)$ it reduces to the Fourier transform of the input signal, whereas the FRFT$(180^o, 180^o)$ leads to self-imaging. For the rest of angles, see Fig. 5, the results are similar (except for scaling) to the ones obtained under Fresnel diffraction of the input signal.

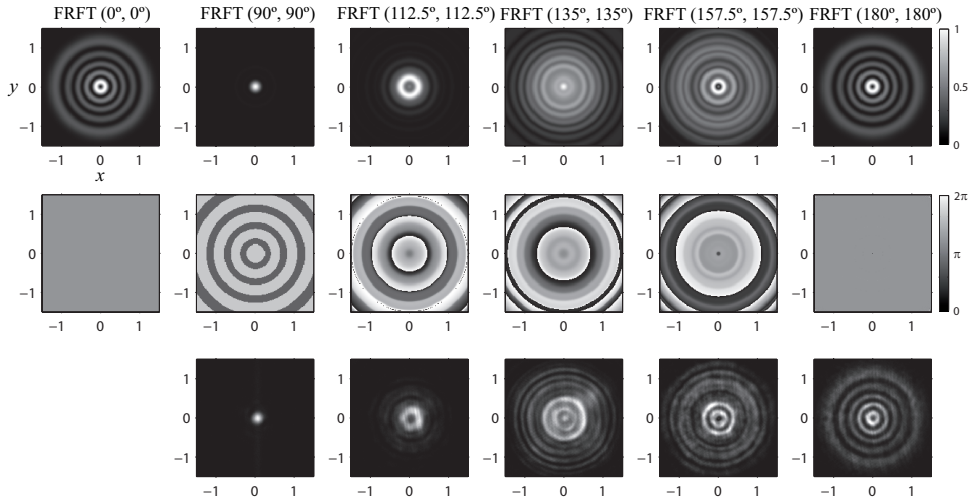

Fig. 5. Transformation of the image $\left|\mathrm{LG}^{+}_{4,1}\right|$ under symmetric FRFT(γ, γ). Numerical simulation (first and second row) and experimental results (third row).

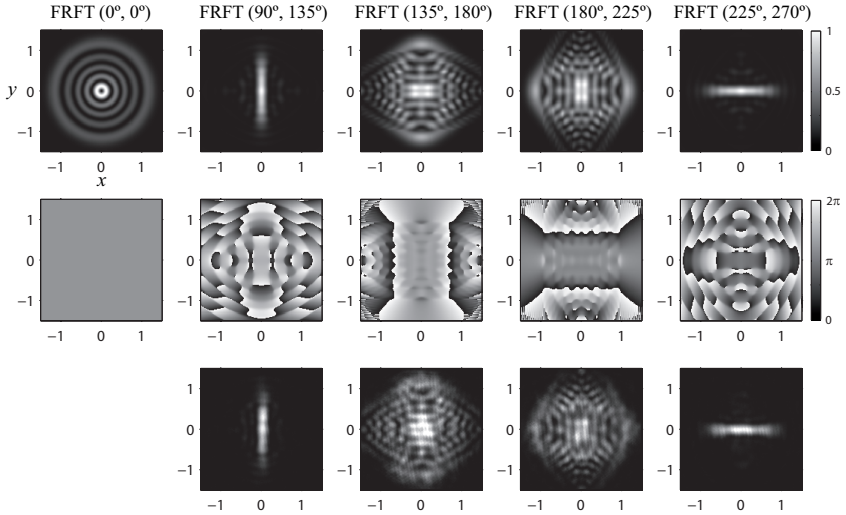

Fig. 6. Transformation of $\left|\mathrm{LG}^{+}_{4,1}\right|$ image under FRFT for $\gamma_y = \gamma_x + k45^o$ with $k = 1, 2, 3$. Numerical simulation (first and second row) and experimental results (third row).

Finally, we study the transformation of $\left|\mathrm{LG}^{+}_{4,1}\right|$ under the FRFT for $\gamma_y = \gamma_x + k45^o$ with $k = 1, 2$ and 3, see Fig. 6. The FRFT(α, γ_y) and FRFT(γ_x, α) when α is set at 90^o and 270^o correspond to the direct/inverse Fourier transforms along the x and y axis, respectively. It is demonstrated in Fig. 6 for the case FRFT$(90^o, 135^o)$ and FRFT$(225^o, 270^o)$. For the rest of

#105474 - $15.00 USD Received 18 Dec 2008; revised 27 Jan 2009; accepted 13 Feb 2009; published 16 Mar 2009

transformation angles intermediate images are obtained, Fig. 6. The comparison of the experimental and numerically simulated results again demonstrates the feasibility of the proposed setup.

The fast modification of the fractional orders allows to implement various proposed algorithms for beam characterization, phase retrieval, information processing, etc. Moreover algorithms such as fractional convolution can be also implemented by using a cascade of optical FRFT setups [1]. Since the last and first lenses corresponding to each FRFT sub-system can be addressed into the same SLM, our setup is also able to perform such operation. Other interesting application is the Radon−Wigner display proposed in [16], which can be used for classification and detection of linear FM components as well as for noise reduction of one-dimensional signals. It contains a continuous representation of the FRFT power spectra of a signal as a function of fractional order. This optical setup also involves fixed free-space intervals but it only performs the one-dimensional FRFT of variable fractional orders.

4. Conclusions

Using two spatial light modulators for lens implementations we have developed an optical setup able to perform automatically the two-dimensional FRFT for an arbitrary set of fractional orders. The variation of the fractional parameter can be done at almost real time. In contrast to other FRFT setups, the resulting transformation has no scaling factors depending on the fractional orders. A setup characterization based on the transformation of HG and LG modes has been demonstrated. The experimental results are in good agreement with the theoretical predictions and demonstrate the setup feasibility for attractive applications such as beam characterization, mode conversion, filtering, phase space tomography, etc.

Acknowledgments

The financial support of the Spanish Ministry of Science and Innovation under projects TEC2005-02180, TEC2008-04105 and Santander-Complutense project PR-34/07-15914 are acknowledged. The authors thank Dr. Oscar Martínez-Matos for valuable discussions.

#105474 - $15.00 USD Received 18 Dec 2008; revised 27 Jan 2009; accepted 13 Feb 2009; published 16 Mar 2009